into liquid ethane chilled by liquid nitrogen, transferred into the JEOL JEM3000SFF cryo-electron microscope[18] and kept at 4.2 K. Low-dose (< 20 electrons per Å^2) images were recorded on Kodak SO163 film at a nominal magnification of ×36,000 and with a 300-kV acceleration voltage. Applied underfocus values were 3.7 to 7.6 μm. Thirty-two images were digitized with a Scitex Leafscan 45 scanner[27] at a pixel size of 2.83 Å at the specimen level. The discernible projection images of the molecule were interactively extracted into 80×80 pixel subframes, and analysed after subtracting the uneven background.

Image analysis

Analysis of images was performed in three major refinement cycles using the Imagic V program system[19]. In the first cycle the selected 11,991 images were first aligned rotationally and translationally, and classified by the reference-free method, and subsequently grouped into 500 clusters by multivariate statistical analysis[28,29]. The resulting averages were used as new references, and the cycle was repeated ten times. In the second cycle, original images were corrected for the contrast transfer function (CTF) of the electron microscope using the parameters Cs 1.6 mm, acceleration voltage 300 kV, Cc 2.2 mm, and aligned with the averages. This further refinement cycle, from the alignment to the generation of references, was repeated eight times. Before the third cycle, orientational Euler angles of the class averages were initially determined from the sinogram[22] of cross-correlation functions assuming a C4 symmetry to obtain a preliminary 3D reconstruction by exact filtered back-projection[30]. For the third cycle, aimed at refining the Euler angles, no symmetry was imposed.

We calculated 189 back-projections in evenly spaced directions from the 3D reconstruction. Each of the 11,991 CTF-corrected images was aligned against all 189 projections and subclustered, providing improved cluster averages, and a new 3D map was generated and projected as above. Again, this cycle was repeated until convergence. The final reconstruction included 11,543 images, 96.3% of the selected images. The isosurface threshold level was chosen to yield an essentially closed surface comprising a total volume of 4×10^5 Å^3. To assess the resolution, independent reconstructions were calculated from two half-sets of the data and assessed by the Fourier shell correlation function[30].

Formation of the channel–antibody complex

The antibody 2B against the carboxy-terminal C19 fragment was prepared as described[13]. Formation of the sodium channel/antibody complex and removal of excessive antibody by gel-permeation chromatography were also carried out as described[13], except that the antibody–sodium channel incubation and gel-permeation buffers were both supplemented with 0.1 M $MgCl_2$ and the incubation with antibody was made for 30 min at 4 °C. Negatively stained samples were recorded, digitized and processed as described[13].

Received 4 September; accepted 22 December 2000.

1. Catterall, W. A. From ionic currents to molecular mechanisms: the structure and function of voltage-gated sodium channels. *Neuron* **26,** 13–25 (2000).
2. McClatchey, A. I. *et al.* Temperature-sensitive mutations in the III–IV cytoplasmic loop region of the skeletal muscle sodium channel gene in paramyotonia congenita. *Cell* **68,** 769–774 (1992).
3. Ptacek, L. J. *et al.* Identification of a mutation in the gene causing hyperkalemic periodic paralysis. *Cell* **67,** 1021–1027 (1991).
4. Deschenes, I. *et al.* Electrophysiological characterization of SCN5A mutations causing long QT (E1784K) and Brugada (R1512W and R1432G) syndromes. *Cardiovasc Res.* **46,** 55–65 (2000).
5. James, W. M. & Agnew, W. S. Multiple oligosaccharide chains in the voltage-sensitive Na^+ channel from *Electrophorus electricus*: evidence for α-2,8-linked polysialic acid. *Biochem. Biophys. Res. Commun.* **148,** 817–826 (1987).
6. Ragsdale, D. S., McPhee, J. C., Scheuer, T. & Catterall, W. A. Molecular determinants of state-dependent block of Na^+ channels by local anesthetics. *Science* **265,** 1724–1728 (1994).
7. Kandel, E. R. & Schwartz, J. H. Molecular biology of learning: modulation of transmitter release. *Science* **218,** 433–443 (1982).
8. Stühmer, W. *et al.* Structural parts involved in activation and inactivation of the sodium channel. *Nature* **339,** 597–603 (1989).
9. Heinemann, S. H., Terlau, H., Stühmer, W., Imoto, K. & Numa, S. Calcium channel characteristics conferred on the sodium channel by single mutations. *Nature* **356,** 441–443 (1992).
10. Vassilev, P. M., Scheuer, T. & Catterall, W. A. Identification of an intracellular peptide segment involved in sodium channel inactivation. *Science* **241,** 1658–1661 (1988).
11. Gordon, R. D., Fieles, W. E., Schotland, D. L., Hogue-Angeletti, R. & Barchi, R. L. Topographical localization of the C-terminal region of the voltage-dependent sodium channel from *Electrophorus electricus* using antibodies raised against a synthetic peptide. *Proc. Natl Acad. Sci. USA* **84,** 308–312 (1987).
12. Rohl, C. A. *et al.* Solution structure of the sodium channel inactivation gate. *Biochemistry* **38,** 855–861 (1999).
13. Sato, C., Sato, M., Iwasaki, A., Doi, T. & Engel, A. The sodium channel has four domains surrounding a central pore. *J. Struct. Biol.* **121,** 314–325 (1998).
14. Doyle, D. A. *et al.* The structure of the potassium channel: molecular basis of K^+ conduction and selectivity. *Science* **280,** 69–77 (1998).
15. Noda, M. *et al.* Primary structure of *Electrophorus electricus* sodium channel deduced from cDNA sequence. *Nature* **312,** 121–127 (1984).
16. Tanabe, T. *et al.* Primary structure of the receptor for calcium channel blockers from skeletal muscle. *Nature* **328,** 313–318 (1987).
17. Tempel, B. L., Papazian, D. M., Schwarz, T. L., Jan, Y. N. & Jan, L. Y. Sequence of a probable potassium channel component encoded at Shaker locus of *Drosophila*. *Science* **237,** 770–775 (1987).
18. Fujiyoshi, Y. The structural study of membrane proteins by electron crystallography. *Adv. Biophys.* **35,** 25–80 (1998).
19. van Heel, M., Harauz, G., Orlova, E. V., Schmidt, R. & Schatz, M. A new generation of the IMAGIC image processing system. *J. Struct. Biol.* **116,** 17–24 (1996).
20. Penczek, P., Radermacher, M. & Frank, J. Three-dimensional reconstruction of single particles embedded in ice. *Ultramicroscopy* **40,** 33–53 (1992).
21. van Heel, M. Classification of very large electron microscopical image data sets. *Optik* **82,** 114–126 (1989).
22. van Heel, M. Angular reconstitution: a posteriori assignment of projection directions for 3D reconstruction. *Ultramicroscopy* **38,** 241–251 (1987).
23. MacKinnon, R. Determination of the subunit stoichiometry of a voltage-activated potassium channel. *Nature* **350,** 232–235 (1991).
24. Miyazawa, A., Fujiyoshi, Y., Stowell, M. & Unwin, N. Nicotinic acetylcholine receptor at 4.6 Å resolution: Transverse tunnels in the channel wall. *J. Mol. Biol.* **288,** 765–786 (1999).
25. Yang, N., George, A. L. Jr & Horn, R. Molecular basis of charge movement in voltage-gated sodium channels. *Neuron* **16,** 113–122 (1996).
26. Liu, Y., Jurman, M. E. & Yellen, G. Dynamic rearrangement of the outer mouth of a K^+ channel during gating. *Neuron* **16,** 859–867 (1996).
27. Mitsuoka, K., Murata, K., Kimura, Y., Namba, K. & Fujiyoshi, Y. Examination of the LeafScan 45, a line-illuminating micro-densitometer, for its use in electron crystallography. *Ultramicroscopy* **68,** 109–121 (1997).
28. van Heel, M. Multivariate statistical classification of noisy images (randomly oriented biological macromolecules). *Ultramicroscopy* **13,** 165–183 (1984).
29. Frank, J., Bretaudiere, J. P., Carazo, J. M., Verschoor, A. & Wagenknecht, T. Classification of images of biomolecular assemblies: a study of ribosomes and ribosomal subunits of *Escherichia coli*. *J. Microsc.* **150,** 99–115 (1988).
30. Harauz, G. & van Heel, M. Exact filters for general geometry three dimensional reconstruction. *Optik* **73,** 146–156 (1986).

Acknowledgements

We thank S. Müller for her illuminating suggestions and help with the manuscript, and M. van Heel, M. Schatz and R. Schmidt for their helpful and constructive advice. T. Moriya promoted the present research. We also thank K. Imoto for discussions, A. Oshima for suggestions and S. Miyazaki for assistance. This work was supported by grants from the ETL, the Japan New Energy and Industrial Technology Development Organization (NEDO), and the Swiss National Science Foundation (to A.E.), and by the Maurice E. Müller Foundation, Switzerland.

Correspondence and requests for materials should be addressed to C.S. (e-mail: tisato@etl.go.jp).

RGS2 regulates signal transduction in olfactory neurons by attenuating activation of adenylyl cyclase III

Srikumar Sinnarajah*, Carmen W. Dessauer†, Deepa Srikumar*, Jun Chen†, John Yuen*, Solomon Yilma‡, John C. Dennis‡, Edward E. Morrison‡, Vitaly Vodyanoy‡ & John H. Kehrl*

** B cell Molecular Biology Section, Laboratory of Immunoregulation, NIAID, NIH, Bethesda, Maryland 20892, USA*
†Department of Integrative Biology and Pharmacology, University of Texas-Houston Medical School, Houston, Texas 77225, USA
‡ Department of Anatomy, Physiology, and Pharmacology, Auburn University, Auburn, Alabama 36849, USA

The heterotrimeric G-protein G_s couples cell-surface receptors to the activation of adenylyl cyclases and cyclic AMP production (reviewed in refs 1, 2). RGS proteins, which act as GTPase-activating proteins (GAPs) for the G-protein α-subunits α_i and α_q, lack such activity for α_s (refs 3–6). But several RGS proteins inhibit cAMP production by G_s-linked receptors[7,8]. Here we report that RGS2 reduces cAMP production by odorant-stimulated olfactory epithelium membranes, in which the α_s family member α_{olf} links odorant receptors to adenylyl cyclase activation[9,10]. Unexpectedly, RGS2 reduces odorant-elicited cAMP production, not by acting on α_{olf} but by inhibiting the activity of adenylyl cyclase type III, the predominant adenylyl cyclase isoform in olfactory neurons. Furthermore, whole-cell voltage clamp recordings of odorant-stimulated olfactory

neurons indicate that endogenous RGS2 negatively regulates odorant-evoked intracellular signalling. These results reveal a mechanism for controlling the activities of adenylyl cyclases, which probably contributes to the ability of olfactory neurons to discriminate odours.

In the nasal cavity, volatile chemicals (odorants) bind seven transmembrane receptors (olfactory receptors) present in the olfactory epithelium, stimulating α_{olf} nucleotide exchange and the dissociation of α_{olf} from the $\beta\gamma$ subunits (refs 9, 10). GTP·α_{olf} binds and activates adenylyl cyclase type III thereby increasing intracellular cAMP levels, which triggers the opening of cyclic-nucleotide-gated cation channels, membrane depolarization, and the generation of action potentials[11,12]. GTP hydrolysis halts α_{olf} signalling and facilitates the re-assembly of the heterotrimeric G_{olf}. As several RGS proteins inhibit signalling through α_s-coupled receptors[7,8], here we examined their effect on α_{olf} signalling.

We measured cAMP production by olfactory epithelium membranes stimulated with odorants in the presence of GTPγS, a non-hydrolyzable form of GTP. Odorants triggered a 15-fold increase in cAMP, whereas similarly prepared respiratory epithelium membranes did not respond (data not shown). Adding recombinant RGS1, RGS2 or RGS3 decreased odorant-induced cAMP production, whereas the addition of two other RGS proteins, RGS4 and RGS5, did not (Fig. 1a). Among the three inhibitory RGS proteins, RGS2 was the most effective: 100 nM RGS2 reduced cAMP production by 50% (Fig. 1b).

As we used GTPγS in these experiments, it is unlikely that RGS2 acted as a GAP for α_{olf}. Also, RGS2 similarly reduced GTPγS·α_s-stimulated cAMP production by olfactory membranes (see below), eliminating the possibility that RGS2 selectively inhibited α_{olf}-triggered production of cAMP. To test whether RGS2 directly blocked α_s from activating adenylyl cyclases, we pre-incubated either GTPγS·α_s or the olfactory membranes with RGS2 before measuring cAMP production. Unexpectedly, pre-incubation of the membranes inhibited cAMP production much more than did pre-incubation of GTPγS·α_s (Fig. 2a). RGS2 seemed to reduce adenylyl cyclase activation independently of any effect on α_s or α_{olf}. Consistent with this possibility, RGS2 inhibited the production of cAMP by olfactory membranes triggered by forskolin (Fig. 2b), an adenylyl cyclase activator that binds at a site distinct from the binding site of GTP·α_s (ref. 2). RGS2 also reduced cAMP production by forskolin- or GTPγS·α_s-treated Sf9 membranes engineered to express adenylyl cyclase type III (Fig. 2c).

Using a similar approach, we determined whether other adenylyl cyclase isoforms shared this sensitivity to RGS2. RGS2 inhibited cAMP production by GTPγS·α_s- or forskolin-stimulated Sf9 membranes expressing type V or VI adenylyl cyclases, but not by those expressing type I or II (Fig. 3a, b). We did not test whether RGS2 inhibits adenylyl cyclase types IV, VII, VIII and IX. Next, using the purified cytoplasmic domains of type V adenylyl cyclase[13], we tested whether RGS2 directly inhibited adenylyl cyclase activity. The addition of purified recombinant RGS2 decreased cAMP production by GTPγS·α_s- or forskolin-stimulated soluble type V adenylyl

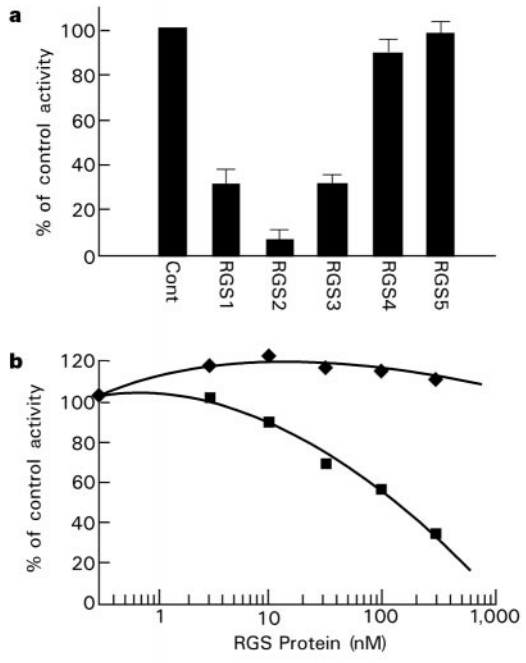

Figure 1 Effects of RGS proteins on adenylyl cyclase activity. **a**, Olfactory membranes were pre-incubated with the indicated RGS proteins (1 μM) and activated with the odorant mixture and GTPγS. cAMP levels from three experiments are expressed as a percentage of the control value (no RGS protein). **b**, Olfactory epithelium membranes were pre-incubated with various concentrations of RGS2 (filled squares) or RGS4 (filled diamonds), and activated with the odorant mixture plus GTPγS. cAMP levels are expressed as a percentage of the control value.

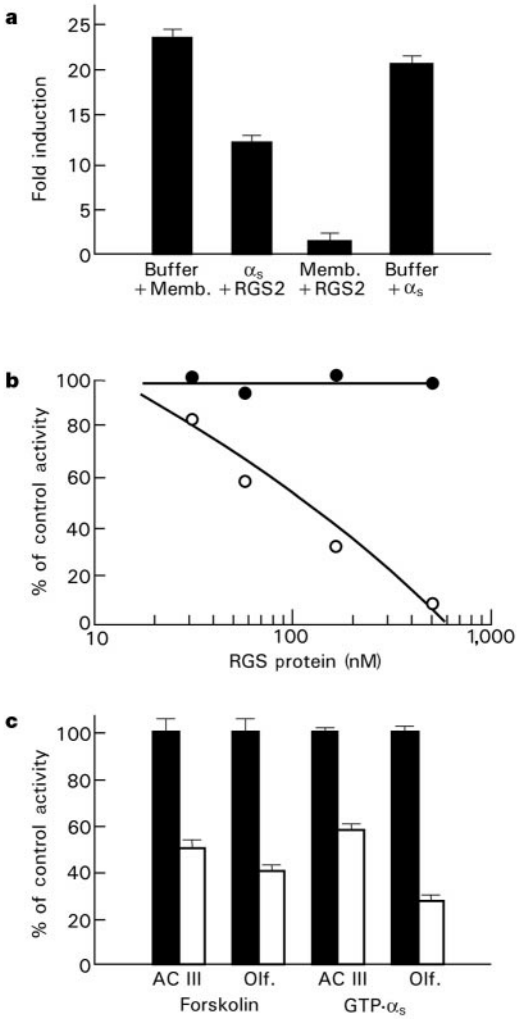

Figure 2 RGS2 inhibits odorant- and forskolin-induced cAMP production. **a**, GTPγS·α_s or olfactory membranes were pre-incubated for 30 min with RGS2 (250 nM) or buffer and then combined with membranes or GTPγS·α_s, respectively. After 5 min cAMP production was measured. **b**, Forskolin (10 μM) stimulated olfactory membranes previously pre-incubated with either RGS2 (filled squares) or RGS4 (filled circles). cAMP levels are expressed as a percentage of the control value (no RGS proteins). **c**, Olfactory membranes (Olf.) or Sf9 membranes expressing type III adenylyl cyclase (AC III) were pre-incubated in the absence (black bar) or presence of 500 nM RGS2 (white bar), and assayed for cAMP production in the presence of GTPγS·α_s or forskolin.

cyclase, whereas the addition of recombinant RGS4 did not (Fig. 3c). Thus, RGS2 directly inhibits the activities of adenylyl cyclase type V, and probably types III and VI, but types I and II are insensitive to RGS2.

To verify that RGS2 inhibits α_s-induced adenylyl cyclase type III activation *in vivo*, we transfected HEK 293 cells with expression vectors for adenylyl cyclase type III and a GTPase-deficient form of α_s, α_sQ227L, in the presence or absence of RGS2. The cellular expression of α_sQ227L causes activation of adenylyl cyclases and cAMP accumulation[14]. Co-expression of RGS2 inhibited the augmented cAMP production that we observed with the addition of adenylyl cyclase III (Fig. 3d); however, RGS2 had little effect on the α_sQ227L-induced cAMP accumulation that occurred without adenylyl cyclase III expression. HEK 293 cells do not express adenylyl cyclase III, but presumably express adenylyl cylase isoforms that are largely insensitive to RGS2.

Because of the pronounced effect of RGS2 on odorant-induced cAMP production, we examined olfactory epithelium for RGS2 expression. We detected RGS2 in olfactory epithelium cell lysates by immunoblot (data not shown) and in most olfactory neuron cell bodies by immunocytochemistry. An antibody specific for olfactory marker protein confirmed the presence of olfactory epithelium, whereas a pre-immune serum showed little reactivity (Fig. 4a–c). Previous immunocytochemical studies detected adenylyl cyclase type III primarily in the apical ciliary layer[15], where a proportion of RGS2 also localized.

Next, we performed whole-cell voltage clamp recordings of olfactory neurons in the presence or absence of the RGS2-specific antibodies. In their absence, odorants elicited characteristic membrane depolarization and repolarization[16], which depended on the applied voltage, whereas cells from the respiratory epithelium did not respond (Fig. 4d, e). When we filled the patch electrode with a solution containing RGS2 antibodies, the odorant-evoked currents changed markedly. Five minutes after beginning the perfusion, we noted a progressive increase in the amplitude of the odorant triggered inward currents (Fig. 4f). The enhancement of odorant-induced inward currents by RGS2 antibodies did not depend on the opening of sodium channels, as the sodium channel blocker tetrodotoxin had no appreciable effect on them (Fig. 4g). Pre-incubation with recombinant RGS2 blocked their enhancement of odorant-induced inward currents (Fig. 4h), indicating that the RGS2 antibodies reacted with endogenous RGS2. In addition, control antibodies had no effect on the odorant-induced inward currents.

Normally, odorants raise intracellular cAMP levels, which opens cyclic nucleotide-gated cation channels resulting in an influx of $Ca^{2+}$and the opening of Ca^{2+}-activated Cl^- channels[17,18]. The diffusion of RGS2 antibodies into olfactory neurons should progressively neutralize RGS2, thereby removing its tempering effect on α_{olf}-stimulated adenylyl cyclase III activity, leading to elevated cAMP levels, opening of additional cyclic-nucleotide-gated channels, and increased inward currents as we observed. An alternative explanation for the increased odorant-elicited inwards currents observed with the RGS2 antibodies is the neutralization of RGS2 α_{olf} GAP activity; however, our biochemical studies do not support this possibility. In addition, the effects of the RGS2 antibody cannot be readily explained by neutralization of RGS2 α_i GAP activity, as this neutralization would be predicted to decrease the inward current.

The sensitivity of adenylyl cyclase III to RGS2 suggests that the constitutive level of RGS2 in olfactory neurons may set a threshold for α_{olf}-mediated signalling. Furthermore, as the two main second messengers generated by odorants, cAMP and Ca^{2+}, both elevate RGS2 messenger RNA expression in other cell types[19,20], RGS2 might

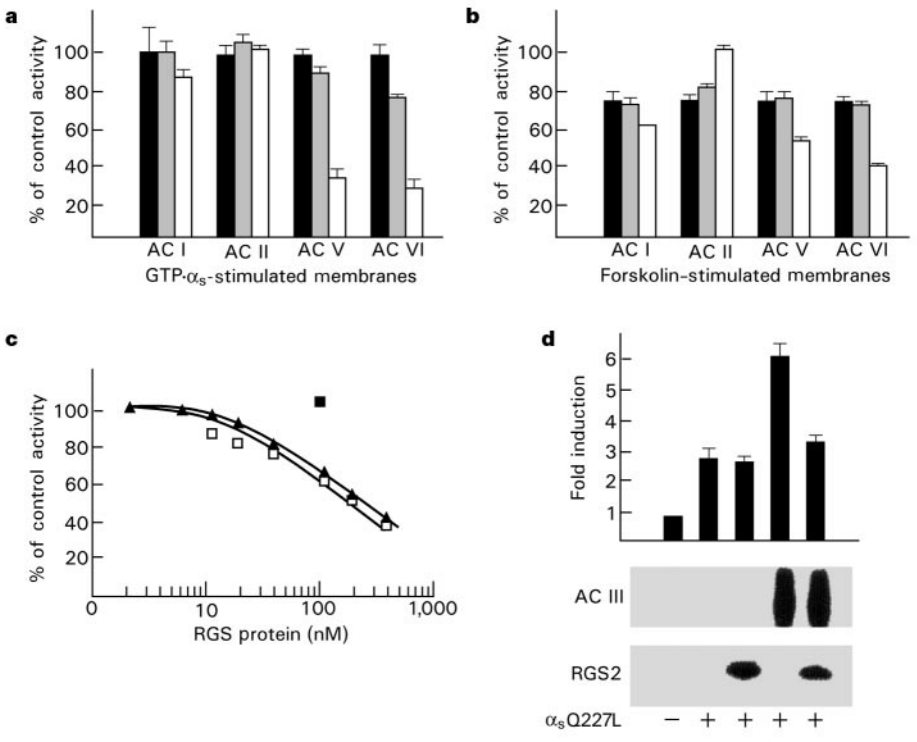

Figure 3 RGS2 inhibits the activity of specific adenylyl cyclases. **a**, **b**, cAMP production by Sf9 membranes expressing the indicated adenylyl cyclase incubated with buffer (black bars), 150 nM (dotted bars) or 500 nM (white bars) RGS2 and stimulated with GTPγS·α_s (**a**) or forskolin (**b**). Data are expressed as a percentage of the control value. **c**, Effect of RGS2 on cAMP production by the C_1 and C_2 domains of adenylyl cyclase type V stimulated with GTPγS·α_s (open squares) or forskolin (filled triangles). Similar assays performed with a single concentration of RGS4 (filled square). **d**, Production of cAMP by HEK 293 cells transfected as indicated with adenylyl cyclase III, α_sQ227L and RGS2. Fold inductions are the mean ± two s.d. of three experiments. Adenylyl cyclase III and RGS2 (HA) levels were assayed by immunoblot.

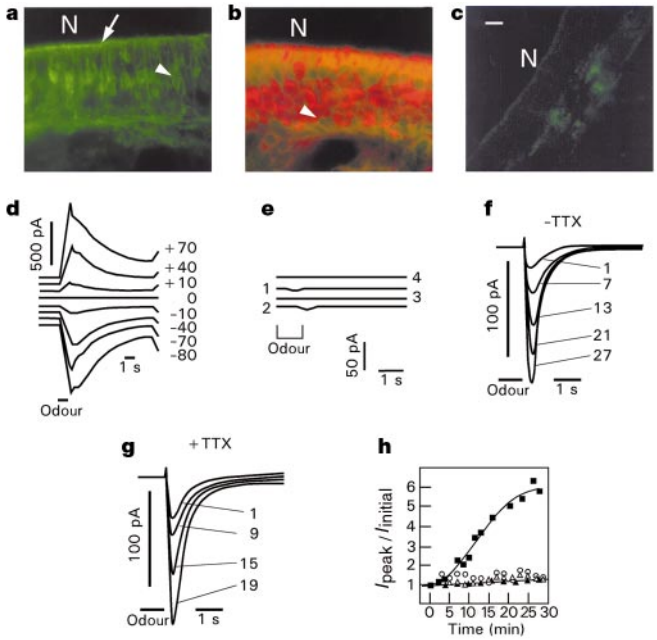

Figure 4 RGS2 attenuates odorant signalling in olfactory neurons. **a–c**, Immunocytochemistry with RGS2-specific antibodies (**a**), or antibodies directed against olfactory marker protein (**b**), or a control (**c**). Arrow in **a** indicates RGS2 expression in the apical ciliary layer. Arrowheads in **a** and **b** delineate individual olfactory neurons. N, nasal cavity. Scale bar, 20 μM. **d**, Current traces from whole-cell voltage recordings of olfactory neurons with holding potentials from –80 to +70 mV. The stimulus was a 1-s pulse of odorant mixture. Downward direction indicates inward current. **e**, Current traces from whole-cell voltage clamp recordings of respiratory epithelium neurons with holding potentials at 0 mV (1) and 90 mV (2), and for patch electrodes contacting a buffer solution with potentials at 0 mV (3) and 60 mV (4). **f**, Odorant-induced currents recorded with patch electrodes filled with RGS2 antibodies (4 μg ml^{-1}). Odorant puffs at 1, 7, 13, 21 and 27 min after initiating the perfusion as indicated. The cell was clamped at –10 mV. **g**, Similar experiment as **f** except that 100 nM tetrodotoxin was added to the buffer solution 5 min before odorant. Odorant puffs at 1, 9, 15 and 19 min after initiating the perfusion. **h**, Plot of normalized, peak negative current ($I_{peak}/I_{initial}$) evoked by odorant versus perfusion time with RGS2 antibody (filled squares), $I_{initial}$ = –22.0 pA; a mixture of RGS2 antibody and RGS2 protein (filled triangles), $I_{initial}$ = –53.2 pA; buffer (open triangles), $I_{initial}$ = –14.3 pA; or anti-olfactory marker protein antibody (open circles), $I_{initial}$ = –94.7 pA.

mediate long-term adaptation to odorants, although perhaps not rapid attenuation, which has been attributed to the phosphorylation and inhibition of adenylyl cyclase by CaM kinase II (ref. 21). In addition, because cardiac myocytes express abundantly two RGS2-sensitive adenylyl cyclase isoforms (types V & VI)[1], cardiac RGS2 expression may temper the positive inotropic effect exerted by β-agonists. □

Methods

Plasmids and antibodies

Expression vectors for the RGS proteins and adenylyl cyclases have been described[1,4]. The αsQ227L expression vector was provided by S. Gutkind (NIH). The anti-HA (haemagglutinin A) and anti-ACIII antibodies were purchased from Covance and Santa Cruz, respectively. The anti-RGS2 antiserum was made in rabbits against a carboxy-terminal peptide (PQITTEPHAT) coupled to keyhole limpet haemocyanin followed by affinity purification using the immunizing peptide. The anti-olfactory marker protein antibody was a gift from F. Margolis (Univ. Maryland School of Medicine).

Transfection of HEK 293 cells

HEK 293 cells were transfected using calcium phosphate with constructs expressing α_sQ227L (0.5 μg per plate), RGS2 (1 μg per plate) and adenylyl cylase III (0.2 μg per plate). The cells were collected 24 h later, and lysates were tested for the production of cAMP (see below). We monitored protein expression by immunoblot.

Olfactory epithelium membrane preparation

We prepared membranes by a modification of published procedures[22]. Dissected rat olfactory epithelium tissues, in EDTA/Ringer's solution containing 2 mM HEPES, 112 mM NaCl, 3.4 mM KCl, 2.4 mM $NaHCO_3$ and 2 mM EDTA, pH7.4, were sonicated for 2 min (Microson tip sonicator at 10 Watts, 23 kHz, at 4 °C under nitrogen gas). The deciliated epithelia were sedimented, and the supernatant centrifuged at 3,000*g* for 5 min and at 146,000 *g* for 30 min, both spins at 4 °C. Purified cilia membrane protein (1 μg) was incubated for 5 min at 37 °C in 50 mM Tris-HCl, 5 mM $MgCl_2$, 20 mM creatine phosphate, 50 units ml^{-1} of creatine kinase and 2 mg ml^{-1} of bovine serum albumin. RGS proteins were pre-incubated with the olfactory epithelium membranes for 30 min at 22 °C. The samples were activated with an odorant mixture (25 μM of equal parts ethyl butyrate, eugenol, and (+) and (–) carvones), α_s·GTPγS, or forskolin for 5 min at 37 °C (all stimulants included 2 mM ATP). The reactions were stopped by boiling, and centrifuged at 13,800*g* for 5 min. cAMP levels were measured by radioimmunoassay (cAMP RIA). Alternatively, boiled lysates from transfected cells were used for the cAMP RIA. Thirty minutes before lysis, the cells were exposed to 1 mM 3-isobutyl-1-methylxanthine in DMEM plus 1% fetal calf serum to inhibit endogenous phosphodiesterases.

Purification of recombinant RGS proteins

Polymerase chain reaction fragments prepared from RGS plasmids were inserted in-frame with hexa-histidine tag in pET15b. IPTG-induced RGS proteins were purified under non-denaturing conditions. The culture of Sf9 (*Spodoptera frugiperda*) cells, and the production, cloning and amplification of recombinant baculoviruses were performed as described[23]. The membranes were collected, washed and re-suspended in 20 mM sodium HEPES, pH 8.0, 2 mM dithiothreitol and 200 mM sucrose.

Purification and assay of C1 and C2 domains

Adenylyl cyclase domains were expressed with an amino-terminal (VC2) or C-terminal (VC1(670)) hexa-histidine tag and purified[13]. Synthesis of cAMP by the C1 and C2 domains was measured at 30 °C for 8–10 min with 1 mM [γ^{32}P]ATP, 5 mM $MgCl_2$ and 50 μM forskolin or 0.4 μM GTPγS·α_s. After quenching the products were separated by sequential chromatography[24]. Activities are expressed per mg of the limiting adenylyl cyclase domain in the assay (C_1). The other domain (C_2) was present in excess (0.5 μM) to drive the interaction between the two proteins.

Immunocytochemistry

Rat ethmoturbinates were fixed with 4% paraformaldehyde, decalcified in 0.25 M EDTA, passed through sucrose solutions of 10%, 20% and 30% placed in plastic moulds that contained Tissue-Tek OCT embedding medium (Sakura) and frozen. Sections (10 μm) were cut, placed on poly-L-coated (Sigma) glass slides, and air dried for 1 h. After washes with distilled H_2O and PBS, the slides were blocked with 10% normal serum and 5% BSA. The primary antibody diluted in the blocking solution was applied overnight, the slides were washed, and Oregon-green-conjugated goat anti-rabbit IgG (1:100; Molecular Probes) or TRITC-conjugated anti-goat IgG (Boehringer Mannheim) was applied for 1 h. The slides were observed through an epi-fluorescence-equipped Nikon Optiphot 2

microscope. Images were captured with a RT-Slider Spot digital camera (Diagnostic Instruments).

Whole-cell voltage clamp recordings

Rat olfactory epithelia were used for whole-cell voltage clamp recordings[25]. Fragments of septal olfactory mucosa were placed in the perfusion chamber such that the basal portions were immersed in physiologic buffer (136.9 mM NaCl, 5.3 mM KCl, 4.2 mM $NaHCO_3$, 0.4 mM KH_2PO_4, 3.4 mM Na_2HPO_4, 5.6 mM D-glucose, pH 7.4), whereas the upper epithelial surfaces with olfactory cilia were exposed to the air. The patch electrode (resistance of 8–16 MΩ) was filled with a solution containing 110 mM KCl, 4 mM NaCl, 2 mM $NaHCO_3$, 1 mM $MgCl_2$, 0.1 mM $CaCl_2$ and 2 mM MOPS at pH 7.4 in the presence or absence of affinity purified RGS2 antibodies (4 μg ml^{-1}), RGS2 antibodies (4 μg ml^{-1}) plus recombinant RGS2 (4 μg ml^{-1}) or control antibodies. After stable contact with an olfactory neuron, 1-s puffs of odorant mixture containing 1.6 mM ethyl butyrate, eugenol and (+) and (−) carvones were applied. The whole-cell response over the time course of several minutes was recorded after being amplified by a voltage-clamp amplifier (Axopatch 200B, Axon Inst.) and filtered at 2–5 kHz. After compensation the series resistance was always lower than 20 MΩ. In some experiments the epithelia were incubated for 5 min in buffer containing tetrodotoxin.

Received 8 August; accepted 4 December 2000.

1. Sunahara, R. K., Dessauer, C. W. & Gilman, A. G. Complexity and diversity of mammalian adenylyl cyclases. *Annu. Rev. Pharmacol. Toxicol.* **36,** 461–480 (1996).
2. Hurley, J. H. Structure, mechanism, and regulation of mammalian adenylyl cyclase. *J. Biol. Chem.* **274,** 7599–7602 (1999).
3. Hepler, J. R. Emerging roles for RGS proteins in cell signaling. *Trends Pharmacol. Sci.* **20,** 376–382 (1999).
4. Kehrl, J. H. Heterotrimeric G protein signaling: roles in immune function and fine-tuning by RGS proteins. *Immunity* **8,** 1–10 (1998).
5. Sunahara, R. K., Tesmer, J. J., Gilman, A. G. & Sprang, S. R. Crystal structure of the adenylyl cyclase activator Gsα. *Science* **278,** 1943–1947 (1997).
6. Natochin, M. & Artemyev, N. O. A single mutation Asp229→Ser confers upon Gsα the ability to interact with regulators of G protein signaling. *Biochemistry* **37,** 13776–13780 (1998).
7. Chatterjee, T. K., Eapen, A. K. & Fisher, R. A. A truncated form of RGS3 negatively regulates G protein-coupled receptor stimulation of adenylyl cyclase and phosphoinositide phospholipase C. *J. Biol. Chem.* **272,** 15481–15487 (1997).
8. Tseng, C. C. & Zhang, X. Y. Role of regulator of G protein signaling in desensitization of the glucose-dependent insulinotropic peptide receptor. *Endocrinology* **139,** 4470–4475 (1998).
9. Schild, D. & Restrepo, D. Transduction mechanisms in vertebrate olfactory receptor cells. *Physiol. Rev.* **78,** 429–466 (1998).
10. Reed, R. R. Signaling pathways in odorant detection. *Neuron* **8,** 205–209 (1992).
11. Pace, U., Hanski, E., Salomon, Y. & Lancet, D. Odorant sensitive adenylate cyclase may mediate olfactory reception. *Nature* **316,** 255–258 (1985).
12. Sklar, P. B., Anholt, R. R. & Synder, S. H. The odorant-sensitive adenylate cyclase of olfactory receptor cells. Differential stimulation by distinct classes of odorants. *J. Biol. Chem.* **261,** 15538–15543 (1986).
13. Dessauer, C. W., Tesmer, J. J., Sprang, S. R. & Gilman, A. G. Identification of a Giα binding site on type V adenylyl cyclase. *J. Biol. Chem.* **273,** 25831–25839 (1998).
14. Landis, C. A. *et al.* GTPase inhibiting mutations activate the alpha chain of Gs and stimulate adenylyl cyclase in human pituitary tumours. *Nature* **340,** 692–696 (1989).
15. Bakalyar, H. A. & Reed, R. R. Identification of a specialized adenylyl cyclase that may mediate odorant detection. *Science* **250,** 1403–1406 (1990).
16. Firestein, S. & Weblin, F. Odor-induced membrane currents in vertebrate olfactory receptor neurons. *Science* **244,** 79–82 (1989).
17. Kleene, S. J. & Gesteland, R. C. Calcium-activated chloride conductance in frog olfactory cilia. *J. Neurosci.* **6,** 3624–3629 (1991).
18. Kurahashi, T. & Taw, K.-W. Co-existence of cationic and chloride components in odorant-induced current of vertebrate olfactory receptor cells. *Nature* **363,** 71–74 (1993).
19. Pepperl, D. J., Shah-Basu, S., VanLeeuwen, D., Granneman, J. G. & MacKenzie, R. G. Regulation of RGS mRNAs by cAMP in PC12 cells. *Biochem. Biophys. Res. Commun.* **243,** 52–55 (1998).
20. Beadling, C., Druey, K. M., Richter, G., Kehrl, J. H. & Smith, K. A. Regulators of G protein signaling exhibit distinct patterns of gene expression and target G protein specificity in human lymphocytes. *J. Immunol.* **162,** 2677–2682 (1999).
21. Wei, J. *et al.* Phosphorylation and inhibition of olfactory adenylyl cyclase by CaM kinase II in Neurons: a mechanism for attenuation of olfactory signals. *Neuron* **21,** 495–504 (1998).
22. Sinnarajah, S. *et al.* Inhibition and enhancement of odorant-induced cAMP accumulation in rat olfactory cilia by antibodies directed against Gαs/olf- and Gαi-protein subunits. *FEBS Lett.* **426,** 377–380 (1998).
23. Summers, M. D. & Smith, G. E. in *Texas Agricultural Experiment Station* Bulletin 1,555 (College Station, Texas, 1987).
24. Salomon, Y., Londos, C. & Rodbell, M. A highly sensitive adenylate cyclase assay. *Anal. Biochem.* **58,** 541–548 (1974).
25. Firestein, S. & Werblin, F. in *Chemical Senses Vol. 1, Receptor Events and Transduction in Taste and Olfaction* (eds Brand, J. G. *et al.*) 449–467 (Marcel Dekker, New York, 1989).

Acknowledgements

We thank M. Rust for editorial assistance; K. Druey, H. Cho and A. Sheschonka for the recombinant RGS proteins; and A. Fauci for support. E.M. and V.V. were supported by grants from the Office of Special Technology, Federal Aviation Administration and Defense Advanced Research Project Agency. C.W.D. was supported by the American Heart Association and the National Institutes of Health.

Correspondence and requests for materials should be addressed to J.K. (e-mail: Jkehrl@niaid.nih.gov).

Recognition of haemagglutinins on virus-infected cells by NKp46 activates lysis by human NK cells

Ofer Mandelboim*, Niva Lieberman*, Marianna Lev†, Lada Paul†, Tal I. Arnon*, Yuri Bushkin‡, Daniel M. Davis§, Jack L. Strominger‖, Jonathan W. Yewdell¶ & Angel Porgador†

** The Lautenberg Center for General and Tumor Immunology, The Hebrew University-Hadassha Medical School, Jerusalem 91120, Israel*
† Department of Microbiology and Immunology, Faculty of Health Sciences, and the Cancer Research Center, Ben Gurion University of the Negev, Beer Sheva 84105, Israel
‡ Laboratory of Molecular Immunology, Public Health Research Institute, 455 First Avenue, New York, New York 10016, USA
§ Department of Biology, Imperial College of Science, Technology and Medicine, London SW7 2AZ, UK
‖ Department of Molecular and Cellular Biology, Harvard University, Cambridge, Massachusetts 01238, USA
¶ Laboratory of Viral Diseases, National Institute of Allergy and Infectious diseases, National Institutes of Health, Bethesda, Maryland

Natural killer (NK) cells destroy virus-infected and tumour cells, apparently without the need for previous antigen stimulation[1]. In part, target cells are recognized by their diminished expression of major histocompatibility complex (MHC) class I molecules, which normally interact with inhibitory receptors on the NK cell surface[2–8]. NK cells also express triggering receptors that are specific for non-MHC ligands; but the nature of the ligands recognized on target cells is undefined[9–14]. NKp46 is thought to be the main activating receptor for human NK cells[9,15]. Here we show that a soluble NKp46–immunoglobulin fusion protein binds to both the haemagglutinin of influenza virus and the haemagglutinin–neuraminidase of parainfluenza virus. In a substantial subset of NK cells, recognition by NKp46 is required to lyse cells expressing the corresponding viral glycoproteins. The binding requires the sialylation of NKp46 oligosaccharides, which is consistent with the known sialic binding capacity of the viral glycoproteins. These findings indicate how NKp46-expressing NK cells may recognize target cells infected by influenza or parainfluenza without the decreased expression of target-cell MHC class I protein.

We studied the role of NKp46 in NK recognition by producing a fusion protein in which the extracellular domain of NKp46 is fused to the Fc portion of immunoglobulin (Ig). Previous reports suggested that NKp46, together with the NKp44 activating receptor, is involved in the lysis of MHC class-I-negative 721.221 cells[12,14,15]. We observed little staining of 721.221 cells when cells were incubated with the NKp46–Ig fusion protein (Table 1). As NK cells can effectively lyse virus-infected cells[1], we tested whether infection with Sendai virus (SV; a mouse paramyxovirus) increased the binding of NKp46–Ig. Remarkably, a 10-fold increase in the staining by NKp46–Ig was observed (Table 1). This effect is specific for NKp46, as SV infection did not alter the binding of other NK receptor–Ig fusion proteins tested (NKAT-8–Ig (KIR2DS4-Ig), KIR-1–Ig (KIR2DL1-Ig), or CD16–Ig; data not shown).

To identify the putative NKp46 ligand, we immunized mice with SV-infected 721.221 cells, and screened spleen-derived B-cell hybridoma supernatants for increased staining of virus-infected cells relative to non-infected cells. The supernatants of one of the hybridoma clones tested (135.7) efficiently blocked the binding of NKp46–Ig to SV-infected cells (Table 1). Enzyme-linked immunosorbent assays (ELISAs) using SV as immunoadsorbent indicated that monoclonal antibody (mAb) 135.7 recognizes a viral gene